วารสารวิทยาศาสตร์บูรพา ปีที่ 27 (ฉบับที่ 2) พฤษภาคม – สิงหาคม พ.ศ. 2565
BURAPHA SCIENCE JOURNAL Volume 27 (No.2) May – August 2022 บทความวิจัย

ฟิล์มโครงสร้างนาโนสังกะสีออกไซด์เตรียมโดยการประยุกต์กระบวนการออกซิเดชันทางความร้อนของฟิล์มสังกะสีที่เคลือบบนผิวรองรับตาข่าย

Nanostructured ZnO Films Prepared by Modified Thermal Oxidation of Zinc Film Deposited on Mesh Substrate

ธงชัย พันธุ์ธาดาพร และ กมล เอี่ยมพนากิจ*

Thongchai Phantadaporn and Kamon Aiempanakit*

ภาควิชาฟิสิกส์ คณะวิทยาศาสตร์และเทคโนโลยี มหาวิทยาลัยธรรมศาสตร์

Department of Physics, Faculty of Science and Technology, Thammasat University

Received : 15 June 2021

Revised : 27 October 2021

Accepted : 12 November 2021

บทคัดย่อ

โครงสร้างระดับนาโนสังกะสีออกไซด์ (ZnO) ถูกเตรียมโดยการเคลือบด้วยไฟฟ้าเคมีบนตาข่ายสแตนเลส (SSM) ด้วยศักย์ไฟฟ้า 4 โวลต์ ใช้อุณหภูมิออกซิเดชัน 300 500 และ 700 องศาเซลเซียส เป็นเวลา 1 ชั่วโมง เพื่อปรับเปลี่ยนโครงสร้างผลึกและสัณฐานวิทยาของฟิล์ม ZnO สมบัติทางสัณฐานวิทยาและโครงสร้างผลึกของฟิล์ม ZnO ได้รับการวิเคราะห์ด้วยกล้องจุลทรรศน์อิเล็กตรอนแบบส่องกราด (FE-SEM) และเครื่องวิเคราะห์การเลี้ยวเบนรังสีเอกซ์ (XRD) ตามลำดับ ผลการวิจัยแสดงให้เห็นว่าฟิล์ม ZnO มีโครงสร้างผลึกแบบเฮกซะโกนอลเวอร์ทไซต์ ขนาดผลึกและความเป็นผลึกสูงขึ้นเมื่อเพิ่มอุณหภูมิออกซิเดชัน ขนาดผลึกใหญ่สุดประมาณ 29.82 นาโนเมตร ที่อุณหภูมิออกซิเดชัน 700 องศาเซลเซียส ฟิล์ม ZnO แสดงสัณฐานวิทยามีลักษณะเป็นแผ่นนาโนมีพื้นผิวที่ไม่ชอบน้ำด้วยมุมสัมผัสหยดน้ำประมาณ 148.2±1.3 องศา ฟิล์ม ZnO ทั้งหมดถูกนำมาทดสอบสมบัติการเร่งปฏิกิริยาด้วยแสงสำหรับการสลายตัวของสารละลายเมทิลีนบลู (MB) ภายใต้การฉายรังสีอัลตราไวโอเลต (UV) ที่เวลาต่าง ๆ ผลการวิจัยพบว่าอุณหภูมิออกซิเดชันมีผลกระทบอย่างมีนัยสำคัญต่อทั้งโครงสร้างผลึกและการเร่งปฏิกิริยาด้วยแสง โดยที่อุณหภูมิออกซิเดชัน 700 องศาเซลเซียส พบว่าฟิล์ม ZnO ให้ผลการสลาย MB ได้ดีที่สุดประมาณ 75.23%

คำสำคัญ : สังกะสีออกไซด์, ออกซิเดชันทางความร้อน, โครงสร้างนาโน, กิจกรรมการเร่งปฏิกิริยาด้วยแสง

Abstract

Zinc oxide (ZnO) nanostructures were prepared by electrochemical deposition on a stainless steel mesh substrate (SSM) at a potential difference of 4 volts. Oxidation temperatures of 300, 500, and 700°C for 1 hour were used to modify the crystal structure and morphology of the ZnO films. The morphological and structural properties of the ZnO films were analyzed with a field emission scanning electron microscope (FE-SEM) and x-ray diffractometer (XRD), respectively. The results indicated that the ZnO films exhibited the crystal structure of hexagonal wurtzite. The crystallinity and crystalline size improved with increasing oxidation temperature. The highest crystalline size of ZnO was about 29.82 nm for an oxidation temperature of 700°C. The ZnO films showed morphology of nanosheet structure with a hydrophobic surface of water contact angle about 148.2° ± 1.3°. All ZnO films were tested for their photocatalytic properties with degradation of methylene blue (MB) solution for various ultraviolet (UV) irradiation time. The results showed that oxidation temperature significantly affected both the crystal structure and photocatalytic activity of ZnO films. The ZnO films prepared at a temperature of 700°C exhibited the best degradation of MB solution of about 75.23%.

Keywords : ZnO, thermal oxidation, nanostructure, photocatalytic activity

***Corresponding author. E-mail** : akamon@tu.ac.th

Introduction

Many materials such as titanium dioxide (TiO_2), tungsten trioxide (WO_3), and zinc oxide (ZnO) exhibit dominant optoelectronic applications including photocatalytic activity, solar cell, or electrochromic device. Among these materials. ZnO is the most widely used material and cheaper than both TiO_2 and WO_3. ZnO is an n-type semiconductor material with a direct and wide bandgap of about 3.37 eV and with a large exciton binding energy of 60 meV at room temperature (Tian *et al*., 2012). Most ZnO show a hexagonal crystal structure which can be used in many applications, including as catalysts (Ong *et al*., 2018), gas sensors (Han *et al*., 2016), optoelectronic devices (Xu *et al*., 2018), UV emitters (Kumari *et al*., 2018), photo-electrochemical device (Desai *et al*., 2019), and solar cells (Ali *et al*., 2016). ZnO has been previously synthesized using various techniques to develop nanostructures such as thermal evaporation (Jouya *et al*., 2020), hydrothermal process (Basnet *et al*., 2020), RF magnetron sputtering (Du *et al*., 2019), physical vapor deposition (Haq *et al*., 2020), and chemical vapor deposition (Chen *et al*., 2010). These techniques require sophisticated equipment and prolonged processing time. The thermal oxidation (TO) process has received great attention since it is an easy, fast, and simple method that does not require complicated equipment or procedures (Ballesteros-Balbuena *et al*., 2020; Rojas-Chávez *et al*., 2020; Wu *et al*., 2018). Moreover, TO can be used to modify the morphology of ZnO nanostructures by varying temperature and oxygen exposure.

In recent years, ZnO has been synthesized by TO from zinc (Zn) powders for photocatalytic applications (Ballesteros-Balbuena *et al*., 2020). The photocatalytic efficiency of ZnO strongly depends on structural properties such as morphology, crystallinity, particle size, and chemical composition. Dikici *et al*. reported that Zn coated on the steel substrate was modified to ZnO by TO with an oxidation temperature of 400 - 800°C and testing photocatalytic activity in MB solution. They found that ZnO at 800°C exhibited nanostructures with the best photocatalytic degradation of MB (Dikici *et al*., 2017). The TO process can be used to prepare nanostructured ZnO film (Rojas-Chávez *et al*., 2020). However, these studies rarely discuss the relationship of oxidation temperature to elemental composition and the relationship of nanostructures for their applications.

In this research, the influence of oxidation temperature on the morphological, structural properties and elemental composition of ZnO films was investigated. Water contact angle (CA) was used to explain the different properties of the prepared surface of nanostructured ZnO films on SSM. Moreover, ZnO films were achieved to test the properties of photocatalytic activity reactions by degrading MB solutions under UV irradiation at different times.

Methods

ZnO films were deposited on a 3x2 cm^2 SSM sheet which was cleaned with an ultrasonic cleaner using deionized water, acetone, and 2-propanol for 15 minutes. The electrochemical method was used to prepare ZnO with a solution of zinc sulfate heptahydrate ($ZnSO_4 \cdot 7H_2O$) at a concentration of 0.05 M and a volume of 50 mL. The SSM was the cathode (-) while the zinc plate was the anode (+). All electrodes were dipped in the $ZnSO_4 \cdot 7H_2O$ solution and adjusted the applied voltage of 4.0 V for 5 minutes. All samples were washed with deionized water and dried in the air. The preparation conditions of the ZnO films on SSM and TO process at various oxidation temperatures are presented in Table 1.

Table1 Deposition and thermal oxidation conditions of ZnO films

Sample	Voltage (V)	Deposition time (min)	Oxidation temperature (°C)	Oxidation time (hr)
1	4	5	-	-
2	4	5	300	1
3	4	5	500	1
4	4	5	700	1

The crystal structure of the ZnO films was determined using the XRD (Bruker D2 Phaser) with Cu-Kα radiation at wavelength of 1.5406 Å (applied voltage of 30 kV, and applied current of 10 mA) which was recorded at 2θ from 20-80° with a step size of 2 °/min. FE-SEM (JEOL 6060) was conducted to study the morphology of the ZnO film. The elemental composition of the sample was analyzed using energy dispersed X-ray spectroscopy (EDX). The methylene blue (MB) solution was used to perform experiments at a concentration of 0.05 mM before irradiation of UV-light to test the photocatalytic activity of the ZnO films. The MB solution was determined the relation between the absorption of the solution and concentration according to Lambert's rules (Swinehart *et al.*,1962; Yu *et al.*, 2002). Absorption of MB was measured via using a spectrophotometer (GENESYS 10S, Thermo Scientific). The distance between the UV light source and MB solution was 100 mm. The UV irradiation was used to test a photocatalytic activity of the ZnO films at a time period in the range of 0 – 120 minutes. Finally, all films were studied the CA by a contact angle goniometer (Rame-Hart Instrument Co. model no. 250-F1) with deionized water about 2μL/drop.

Results

The crystal structure and crystallinity of ZnO films affected the photocatalytic performance. Figure 1 shows the XRD results of bare SSM and deposited ZnO films on SSM. It was found that bare SSM showed XRD peaks at 2θ of 43.8°, 44.7°, 51.1°, and 74.9° corresponding with the (111), (110), (200), and (220) planes of stainless steel with face center cubic structure. As-deposited films on SSM exhibited an XRD peak at 2θ of 37.0° corresponding to given index value (101) while at 2θ of 39.3°, 43.5°, and 54.4° exhibited the Zn of the (100), (101), and (102) planes (PDF number: 00-001-1244), respectively. The thermally oxidized ZnO films showed that XRD intensity enhanced with increased oxidation temperatures from 300 to 700°C. This indicates that the hexagonal wurtzite structure of the crystallinity of ZnO improved as 2θ of 31. 9°, 34.6°, 36.4°, 47.8°, 56.9°, 63.2°, 66.7°, and 69.5° corresponding with (100), (002), (101), (102), (110), (103), (200), and (201) planes (PDF number: 01-082-3143), respectively. The crystallite size of ZnO at the highest intensity peak of (101) was 19.79, 14.71, and 29.82 nm at oxidation temperature of 300, 500, and 700°C, respectively, which can be calculated by using the Scherrer equation (Yuan *et al*., 2013) as shown in Equation (1).

$$D = 0.9\lambda/\beta\cos\theta \quad (1)$$

where D is the crystallite size, K = 0.9 (Scherrer constant), λ = 0.15406 nm (wavelength of the x-ray sources), β is the full width at half maximum (FWHM) of the diffraction peak, and θ is the Bragg angle (radians).

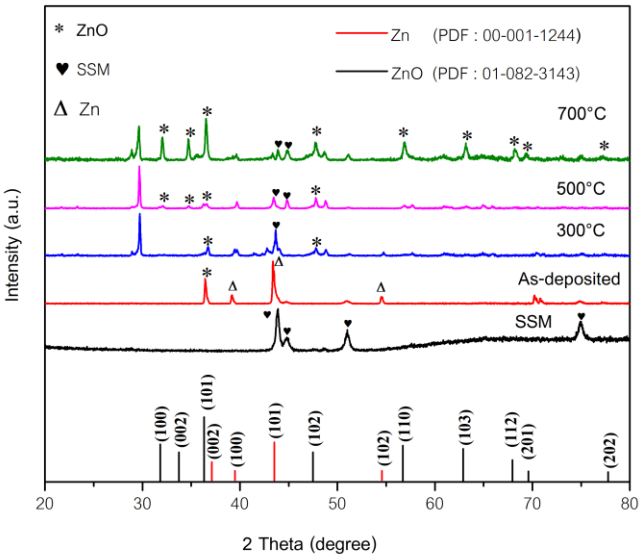

Figure 1 XRD patterns of the sample for SSM, as-deposited, and ZnO films at different oxidation temperatures.

Figure 2 shows FE-SEM image of a) bare SSM and b) - e) deposited ZnO on SSM. The surface of SSM exhibited a rough and smooth grooved surface while the surface of as-deposited films showed the structure of 2 dimension (2D) nanosheet on micro-grain (Fig. 2 b) due to the reaction of $ZnO_4 \cdot 7H_2O$ during the electrochemical process (Dikici *et al.*, 2017). Usually, ZnO occurs from Zn by TO at temperatures of 450-700°C (Zhao *et al.*, 2013; Khanlar *et al.*, 2012; Altaweel *et al.*, 2017; Arafat *et al.*,2020) which is associated with Zn liquids and vapor phases. Since Zn has a melting point of 419.5°C (Yuan *et al.*, 2013), the growth mechanism of ZnO nanostructures is controlled by vapor-liquid-solid (VLS) catalysis (Khanlary *et al.*, 2012). Figure 2 c)-e) shows the influence of oxidation temperature on the morphology of ZnO nanostructures which changes from a dense nanosheet to a porous nanosheet. The structural properties of ZnO depend on the TO and time were exhibited (Ballesteros-Balbuena *et al.*, 2020; Rojas-Chávez *et al.*, 2020; Wu *et al.*, 2018) and that improved the quality of ZnO. Figure 2 e) at an oxidation temperature of 700°C, the morphology of ZnO films was a porous nanosheet and the same as the disordered nanotube structure. Therefore, the surface area of ZnO was enhanced with increasing oxidation temperature.

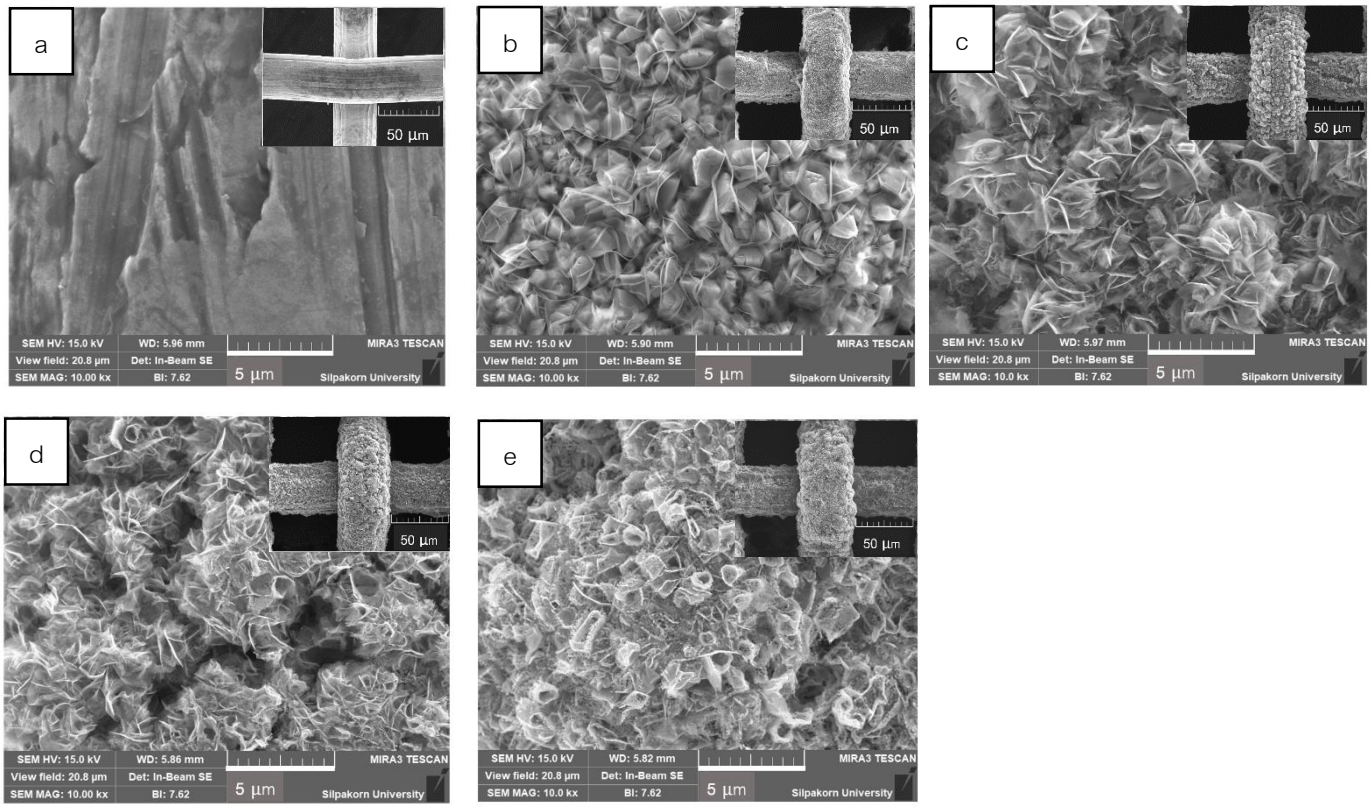

Figure 2 FE-SEM image of a) SSM, b) as-deposited, ZnO film at oxidation temperatures of c) 300, d) 500, and e) 700°C.

After analyzing to identify the elemental composition with the EDX technique as shown in Figure 3, we found that the SSM comprised three major Fe, Cr, and Ni elements while deposited ZnO on SSM showed major Zn and O elements. Figure 3 (b) shows the relationship of the elemental composition of as-deposited ZnO and thermally oxidized ZnO at oxidation temperatures of 300, 500, and 700°C. The as-deposited ZnO without TO was found to exhibit Zn of 64.81 at% and O of 29.66 at%. The O in the films increased after the TO and turned to that decrease of Zn proportion with the rearrangement of the atom. It was found that Zn and O were in the range of 50-65% and 29-45%, respectively. Almost 50% of the O content was obtained which corresponded with the findings of (Jouya *et al.*, 2020).

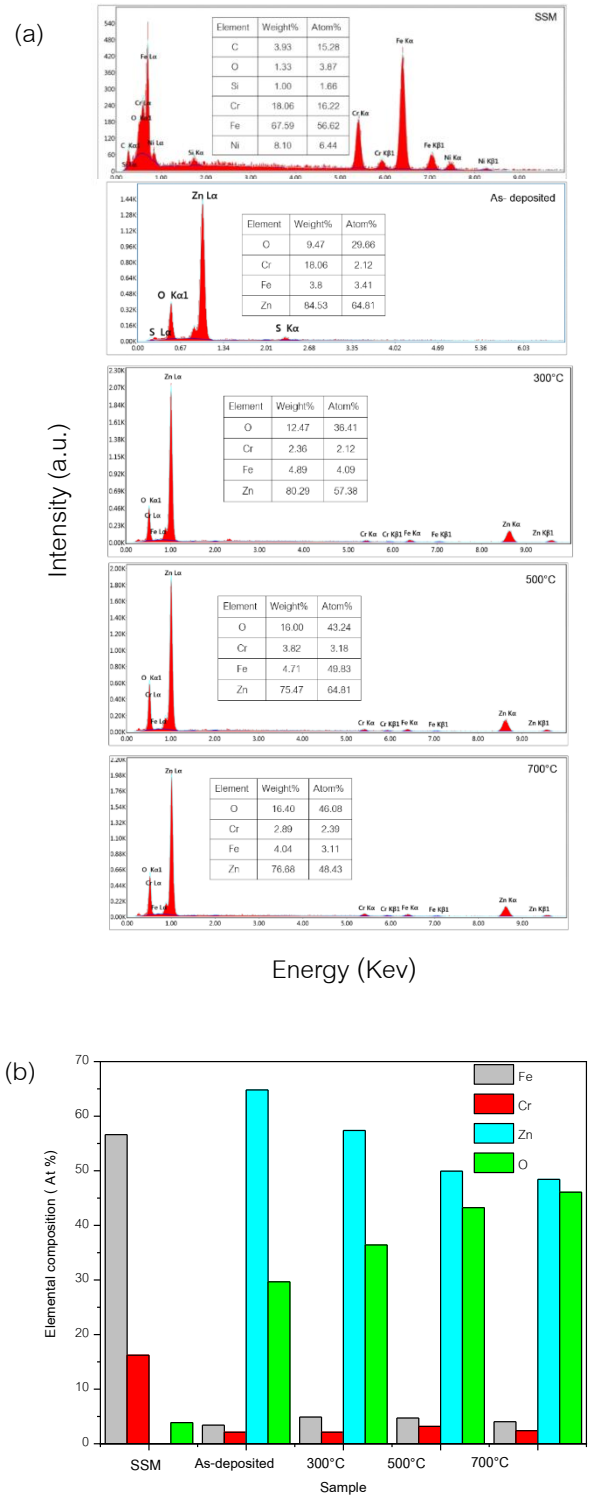

Figure 3 Analysis of EDX spectra of all samples (a) elemental spectrum and (b) the relationship of elemental composition.

Before testing the photocatalytic properties, a linear equation between the concentration of MB solution and absorbance must be created with the optimum absorbance at a wavelength of 664 nm. The absorbance values of 0.3370, 0.6775, 1.0413, 1.4699, and 1.6352 corresponded with MB concentrations of 0.01, 0.02, 0.03, 0.04, and 0.05 mM, respectively. The linear relationship between absorbance and MB concentration according to Lambert-Beer rules (Yu *et al.*, 2002) provide a linear equation y = 0.03411X and R^2 = 0.99019, where x, y, and R^2 are MB concentrations, absorbance at wavelength of 664 nm, and the square of the correlation coefficient, respectively, as shown in Figure 4.

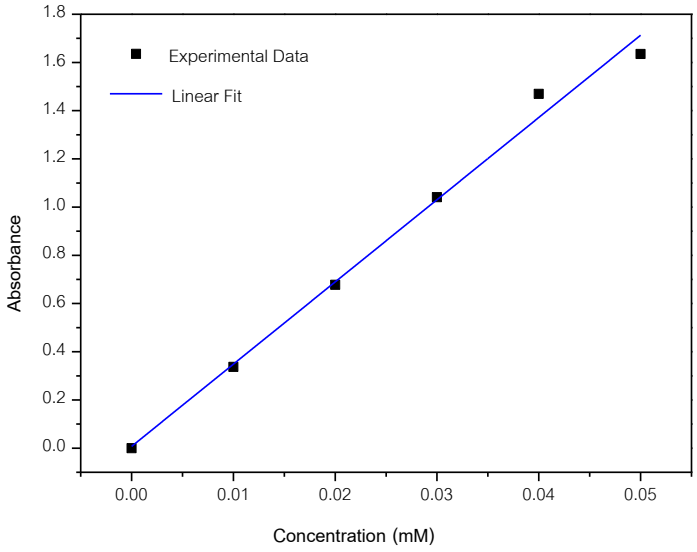

Figure 4 Standard curves between absorbance and concentrations of MB solution at 0.01, 0.02, 0.03, 0.04, and 0.05 mM.

The photocatalytic degradation process is due to the action of hydroxyl radicals formed during the reaction. The mechanism of degradation occurred when the ZnO nanosheet was irradiated with UV (photon energy (h**ν**), electrons (e^-) excited from the valence band to the conduction band. The hydroxyl group on the surface of the ZnO nanosheet reacts with the holes (h^+) to form hydroxyl radicals ($OH^•$). Additionally, dissolved oxygen reacts with electrons to form peroxides (O_2^-). This peroxide takes one and two protons to form superoxide (O_2^-) and hydrogen peroxide (H_2O_2), respectively (see Equations 2 - 7). These reactive radicals react with MB and degrade them into non-toxic organic compounds (Ridhuan *et al.*, 2012).

$$ZnO + h\nu \rightarrow ZnO + e^- + h^+ \quad (2)$$

$$OH^- + h^+ \rightarrow OH^\bullet \quad (3)$$

$$O_2 + e^- \rightarrow O_2^- \quad (4)$$

$$O_2^- + H^+ \rightarrow HO_2 \quad (5)$$

$$2HO_2 \rightarrow H_2O_2 + O_2 \quad (6)$$

$$H_2O_2 + e^- \rightarrow OH^- + OH^- \quad (7)$$

Figure 5 shows photocatalytic decolorization of MB with and without ZnO films under UV irradiation. The photocatalytic activity can be expressed as C/C_0, where C_0 is the initial concentration of MB and C is the MB concentration after UV-light irradiation. The degradation of MB for samples in the dark (without UV irradiation and ZnO) and MB under UV irradiation (without ZnO) showed a slow decrease of C/C_0, while the samples with ZnO under UV irradiation exhibited a rapid decrease as oxidation temperature increased. Therefore, TO plays an important role in the degradation of MB in photocatalytic of ZnO films. Enhanced degradation of MB is due to the higher surface area and greater crystallinity of the films. These reasons were described with the thermodynamic model to improve the properties of films (Leitner *et al.*, 2018; Sahu *et al.*, 2009; Fan *et al.*, 2011). In this study, the best sample of degradation of MB was ZnO films at thermal oxidation of 700°C which can be formed on SSM substrate with a porous nanosheet structure. The surface defects prevented electron and hole aggregation and resulted in increased radicals (Demirci *et al.*, 2015).

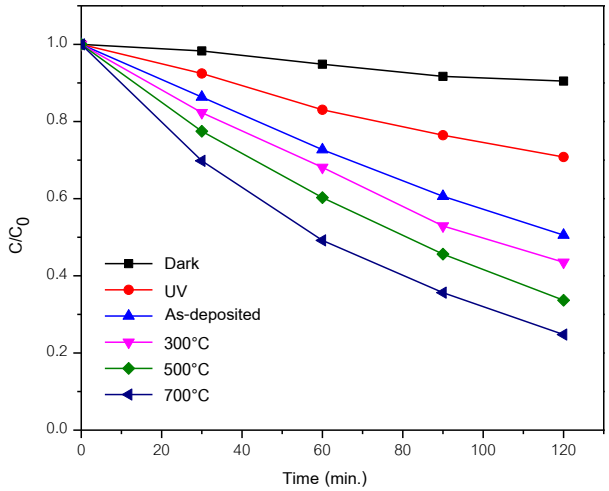

Figure 5 Photocatalytic of the ZnO films for the degradation of MB solution at different UV irradiation durations.

The change in $\ln(C_0/C)$ with the time under irradiation is shown in Figure 6 for oxidation temperatures of 300, 500, and 700°C. The graph of $\ln(C_0/C)$ with the irradiation period showed a straight line as Eq. (8) with the decomposition rate constant where k is the slope and optical decolorization kinetics are consistent with a first-order kinetic reaction.

$$\ln(C_0/C) = kt \qquad (8)$$

Samples of ZnO nanosheet with an oxidation temperature at 700°C, as-deposited, and MB in the dark exhibited the value of k at 0.0163, 0.0056, and 0.0008 min^{-1}, respectively, in which the ZnO nanosheet was faster than as-deposited and MB stored in the dark by 2.91 and 20.38 times, respectively.

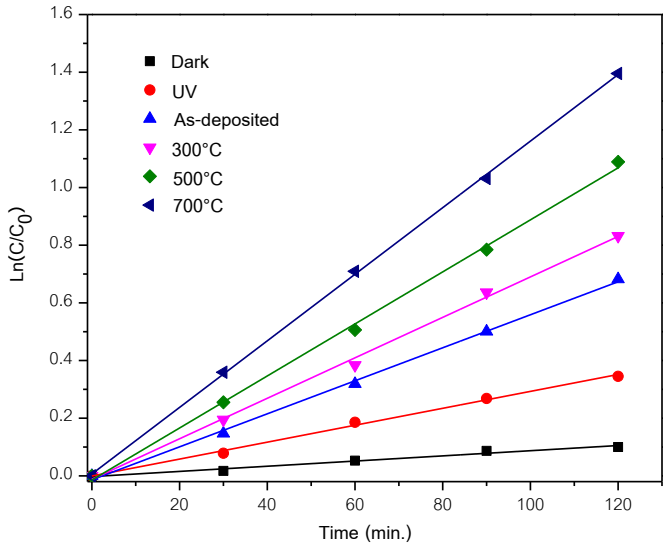

Figure 6 Kinetic reaction of all samples.

Figure 7 shows the degradation of MB as calculated from Eq. (9) for all conditions. Oxidation temperatures of 300, 500, and 700°C exhibited degradation of 58.47, 66.34, and 75.23%, respectively. The results show significant effects of the MB degradation under UV irradiation with using ZnO nanosheet. The relationships of surface morphology, crystallinity, and oxygen content with oxidation temperature agree well with optimizing the photocatalytic activity of ZnO films.

$$\text{Degradation of MB (\%)} = \frac{C_0 - C}{C_0} \times 100 \quad (9)$$

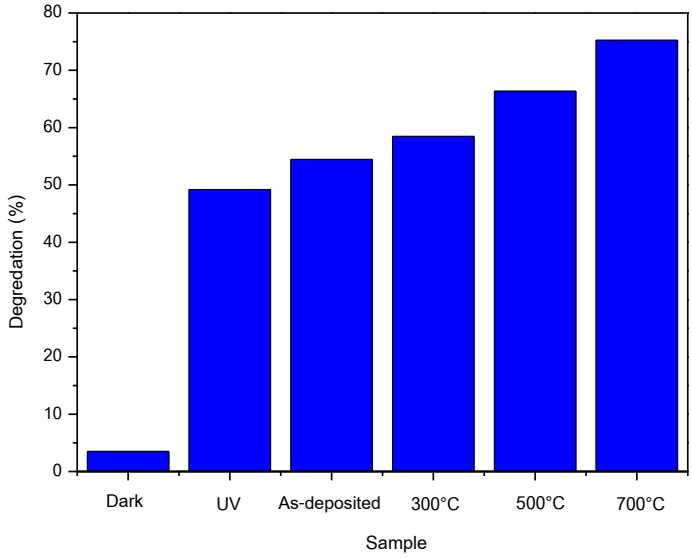

Figure 7 Photocatalytic degradation of MB solution for all conditions.

Finally, the study of polar properties using CA when water droplets are on the surface of films and without the spread of water droplets remains shaped and angled to surfaces. These are described by surface tension between the liquid-solid, liquid-air, and solid-air so that a balanced CA measures the ability of liquids to wet solids. The associated surface tension can be explained by Young's equation (Li *et al*., 2018). Two characteristics of water droplets on solid surfaces are hydrophilic surfaces ($0° < \theta < 90°$) and hydrophobic surfaces ($90° < \theta < 180°$) where θ is CA (Pereira *et al.*, 2015). Figure 8. shows water droplets on the surface of SSM and ZnO films. The result confirms that the nanosheet structure of ZnO films enhanced the CA as the oxidation temperature increased.

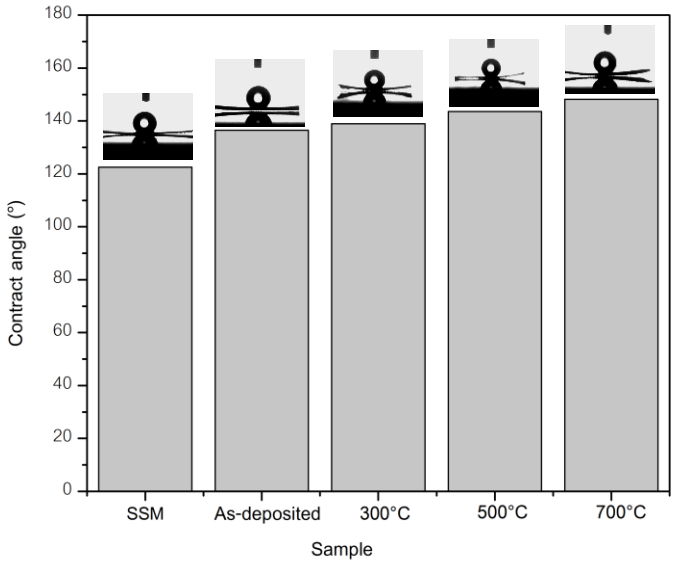

Figure 8 Water contact angle of SSM and different ZnO films.

Discussion

The nanostructured ZnO films were prepared by electrodeposition on SSM and modified structure with TO at oxidation temperatures of 300, 500, and 700°C for 1 hour. The ZnO films exhibited a nanosheet structure with the highest crystallite size of approximately 29.82 nm when oxidation temperature increased to 700°C. TO enhanced the crystallinity of ZnO films and improved the oxygen content in ZnO films. Nanostructured ZnO films were modified from dense nanosheet to porous nanosheet. In addition, the photocatalytic reaction of ZnO films showed the best sample when oxidation temperatures increased to 700°C with degradation of the MB solution at 75.23%. The reasons for the high degradation of MB were increasing crystallinity and an enhanced active surface area of ZnO films (see Figures 1 and 2). Furthermore, the ZnO films were tested for CA which obtained hydrophobic CA at about 148.2° ± 1.3°. The geometrical structure of the surface and the surface energy are two main factors that affect the wetting properties directly (Kobina Sam *et al.*, 2019). Beside, creating hierarchical dual-scale structures has an essential role in obtaining the special wettability relating to the Cassie-Baxter state (Velayi *et al.*, 2017). These results are due to the modified structure which mentions by the mechanism of the growth of ZnO nanostructures with vapor-liquid-solid (VLS) catalysis (Khanlary *et al.*, 2012) at high oxidation. However, this research has a percentage of degradation of less than 90% when compared to other studies that the same conditions showed a

better percentage of degradation (Dikici *et al*., 2017) and a higher CA according to the oxidation temperature from the above conditions.

Conclusions

Nanostructured ZnO films were deposited with an electrodeposited on SSM substrate which modified the structure via TO at various oxidation temperatures of 300, 500, and 700°C for 1 hour. The results indicate that increased oxidation temperature improved the crystal structure with high crystallinity and large crystallite size. ZnO films exhibited the morphology of a nanosheet which modified from a dense nanosheet to a porous nanosheet by TO. Moreover, we found that the photocatalytic activity of ZnO films increased with oxidation temperature. AN oxidation temperature of 700°C indicated the highest degradation of the MB solution and CA of water at 75.23% and 148.2° ±1.3°, respectively.

Acknowledgements

The authors would like to thank the Faculty of Science and Technology, Thammasat University for the provision of research facilities. The authors gratefully acknowledge funding from the Faculty of Science and Technology, Thammasat University Research Fund (Contract No. SciGR31/2563). The authors would also like to thank the Nation Electronics and Computer Technology Center (NECTEC) for providing experimental facilities.

References

Ali, N., Hussain, A., Ahmed, R., Wang, M. K., Zhao, C., Haq, B. U., & Fu, Y. Q. (2016). Advances in nanostructured thin film materials for solar cell applications. *Renewable and Sustainable Energy Reviews*, *59,* 726–737.

Altaweel, A., Imam, A., Ghanbaja, J., Mangin, D., Miska, P., Gries, T., & Belmonte, T. (2017). Fast synthesis of ultrathin ZnO nanowires by oxidation of Cu/Zn stacks in low-pressure afterglow. *Nanotechnology*, *28*(8), 085602.

Arafat, M. M., Rozali, S., Haseeb, A. S. M., & Ibrahim, S. (2020). Direct and catalyst-free synthesis of ZnO nanowires on brass by thermal oxidation. *Nanotechnology*, *31*, 12344.

Basnet, P., & Chatterjee, S. (2020). Structure-directing property and growth mechanism induced by capping agents in nanostructured ZnO during hydrothermal synthesis - A systematic review. *Nano-Structures & Nano-Objects*, *22*, 100426.

Ballesteros-Balbuena, M., Roa-Morales, G., Vilchis-Nestor, A. R., Castrejón-Sánchez, V. H., Vigueras-Santiago, E., Balderas-Hernández, P., & Camacho-López, M. (2020). Photocatalytic urchin-like and needle-like ZnO nanostructures synthetized by thermal oxidation. *Materials Chemistry and Physics*, 122703.

Chen, Z., Shum, K., Salagaj, T., Wei Zhang, & Strobl, K. (2010). ZnO thin films synthesized by chemical vapor deposition. 2010 IEEE Long Island Systems, Applications and Technology Conference.

Demirci, S., Ozturk, B., Yildirim, S., Bakal, F., Erol, M., Sancakoglu, O., Yigit, R., Celik, E., & Batar, T. (2015). Synthesis and comparison of the photocatalytic activities of flame spray pyrolysis and sol-gel derived magnesium oxide nano-scale particles. *Materials Science in Semiconductor Processing*, *34*, 154–161.

Dikici, T. (2017). Temperature-dependent growth of ZnO structures by thermal oxidation of Zn coatings electrodeposited on steel substrates and their photocatalytic activities. *Ceramics International*, *43*(11), 8289–8293.

Du, B., Jiang, J., Li, J., & ZHU, W. (2019). Effects of ZnO Magnetron Sputtering on Surface Charge and Flashover Voltage of Oil-impregnated Paper. *High Voltage*, *4*, 308-315.

Desai, M. A., Sharma, V., Prasad, M., Jadkar, S., Saratale, G. D., & Sartale, S. D. (2019). Seed-layer-free deposition of well-oriented ZnO nanorods thin films by SILAR and their photoelectrochemical studies, *International Journal of Hydrogen Energy*, *45*, 5783-5792.

Fan, G., Huang, Z., Jiang, J., & Sun, L. (2011). Standard molar enthalpy of formation of the ZnO nanosheets. *Journal of Thermal Analysis and Calorimetry*, *110*(3), 1471–1474.

Han, B., Liu, X., Xing, X., Chen, N., Xiao, X., Liu, S., & Wang, Y. (2016). A high response butanol gas sensor based on ZnO hollow spheres. *Sensors and Actuators B: Chemical*, *237,* 423–430.

Haq, I. ul, Jacob, J., Mehboob, K., Mahmood, K., Ali, A., Amin, N., & Ashraf, F. (2020). Effect of annealing temperature on the thermoelectric properties of ZnInO thin films grown by physical vapor deposition. *Physica B: Condensed Matter*, 412569.

Jouya, M., Taromian, F., & Afshari Abolkarlou, M. (2020). Growth of Zn thin films based on electric field by thermal evaporation method and effect of oxidation time on physical properties of ZnO nanorods, *Journal of Materials Science: Materials in Electronics*, *31,* 321.

Khanlary, M. R., Vahedi, V., & Reyhani, A. (2012). Synthesis and Characterization of ZnO Nanowires by Thermal Oxidation of Zn Thin Films at Various Temperatures. *Molecules*, *17*(5), 5021–5029.

Kumari, C., Pandey, A., & Dixit, A. (2018). Zn interstitial defects and their contribution as efficient light blue emitters in Zn rich ZnO thin films. *Journal of Alloys and Compounds*, *735*, 2318–2323.

Kobina Sam, E., Kobina Sam, D., Lv, X., Liu, B., Xiao, X., Gong, S., & Liu, J. (2019). Recent development in the fabrication of self-healing superhydrophobic surfaces. *Chemical Engineering Journal*, *373*, 531–546.

Leitner, J., Bartunek, V., Sedmidubsky, D., & Jankovsky, O. (2018). Thermodynamic properties of nanostructured ZnO. *Applied Materials Today*, *10,* 1–11.

Li, F., Wang, Z., Huang, S., Pan, Y., Zhao, X. (2018). Flexible, Durable, and Unconditioned Superoleophobic/Superhydrophilic Surfaces for Controllable Transport and Oil-Water Separation. *Advanced Functional Materials*, *28*(20), 1706867.

Ong, C. B., Ng, L. Y., & Mohammad, A. W. (2018). A review of ZnO nanoparticles as solar photocatalysts: Synthesis, mechanisms and applications. *Renewable and Sustainable Energy Reviews*, *81,* 536–551.

Pereira, M.M., Kurnia, K.A., Sousa, F.L., Silva, N.J.O., Lopes-da-Silva, J.A., Coutinho, J.A.P., & Freire, M.G. (2015). Contact angles and wettability of ionic liquids on polar and non-polar surfaces. *Physical Chemistry Chemical Physics*,*17*(47), 31653–31661.

Ridhuan, N. S., Abdul Razak, K., Lockman, Z., & Abdul Aziz, A. (2012). Structural and Morphology of ZnO Nanorods Synthesized Using ZnO Seeded Growth Hydrothermal Method and Its Properties as UV Sensing. *PLOS ONE*, *7*(11), e50405.

Rojas-Chavez, H., Cruz-Martínez, H., Montejo-Alvaro, F., Farías, R., Hernandez-Rodriguez, Y. M., Guillen-Cervantes, A., & Cigarroa-Mayorga, O. E. (2020). The formation of ZnO structures using thermal oxidation: How a previous chemical etching favors either needle-like or cross-linked structures. *Materials Science in Semiconductor Processing*, *108*, 104888.

Sahu, D.R., Hong, L.Y., Wang, S.C., & Huang, J.L. (2009). Synthesis, analysis and characterization of ordered mesoporous /SBA-15 matrix: effect of calcination temperature. *Microporous Mesoporous Mater*, *117,* 640–649.

Starkweather, B.A., Zhang, X., & Counce, R.M. (2000). An Experimental Study of the Change in the Contact Angle of an Oil on a Solid Surface. *Industrial & Engineering Chemistry Research*, *39*(2), 362–366.

Swinehart, D. F. (1962). The Beer-Lambert Law, *Journal of Chemical Education*, Vol.*39*(7), 333.

Tian, C., Zhang, Q., Wu, A., Jiang, M., Liang, Z., Jiang, B., & Fu, H. (2012). Cost-effective large-scale synthesis of ZnO photocatalyst with excellent performance for dye photodegradation. *Chemical Communications*, *48*(23), 2858.

Velayi, E., & Norouzbeigi, R. (2017). Robust superhydrophobic needle-like nanostructured ZnO surfaces prepared without post chemical-treatment. *Applied Surface Science*, *426*, 674–687.

Wallace, I., Eshu, O. V., Chukwunonso, O. B. & Okoro, U. C. (2015). Synthesis and Characterization of Zinc Oxide (ZnO) Nanowire. *Journal of Nanomedicine & Nanotechnology*, *06*(05).

Wu, F., Wang, C., Wu, M., Vinodgopal, K., & Dai, G.-P. (2018). Large Area Synthesis of Vertical Aligned Metal Oxide Nanosheets by Thermal Oxidation of Stainless Steel Mesh and Foil. *Materials*, *11*(6), 884.

Xu, L., Miao, J., Chen, Y., Su, J., Yang, M., Zhang, L., & Ding, S. (2018). Characterization of Ag-doped ZnO thin film for its potential applications in optoelectronic devices. *Optik*, *170*, 484–491.

Yu, J. C., Yu, Ho, Jiang, & Zhang. (2002). Effects of F-Doping on the Photocatalytic Activity and Microstructures of Nanocrystalline TiO_2 Powders. Chemistry of Materials, *14*(9), 3808–3816.

Yuan, L., Wang, C., Cai, R., Wang, Y., & Zhou, G. (2013). Spontaneous ZnO nanowire formation during oxidation of Cu-Zn alloy. *Journal of Applied Physics*, *114*(2), 023512.

Zhao, C. X., Li, Y. F., Zhou, J., Li, L. Y., Deng, S. Z., Xu, N. S., & Chen, J. (2013). Large-Scale Synthesis of Bicrystalline ZnO Nanowire Arrays by Thermal Oxidation of Zinc Film: Growth Mechanism and High-Performance Field Emission. *Crystal Growth & Design*, *13*(7), 2897–2905.